

Mediating scale separation in Strongly Coupled Data Assimilation

Avneet Singh^{1, 2, 3†}, Alberto Carrassi^{1, 2, 3}, Francois Counillon^{1, 2, 3}

¹ The Geophysical Institute, University of Bergen, Bergen 5007, Norway

² The Nansen Environmental and Remote Sensing Center, Thormøhlens gate 47, Bergen 5006, Norway

³ Bjerknes Centre for Climate Research, University of Bergen, Bergen 5007, Norway

Abstract

Data Assimilation (DA) in a simple coupled system set-up is explored using linear and non-linear coupled toy models capturing the macroscopic properties of the ocean-atmosphere interactions. We especially concentrate on the effects of temporal scale separation between the oceanic and atmospheric sub-components, and its effects on the optimal implementation and possible modifications at the zeroth order to the typical DA procedures employed in weather forecasting and climate prediction.

1 Introduction

Data Assimilation (*abbrev.* DA), broadly speaking, is a conceptual and mathematical framework that aims to combine the information from observational datasets with the predictions from proposed model forms in order to yield a ‘true’ estimate of the state; the ‘true’ state in this case refers to the derived state that is a more accurate representation of the system than what is predicted by the model, or implied by the observations, independently. In some sense, DA could be interpreted as a propagation of an initial forecast state predicted by a given model towards higher likelihood by *assimilating* the observations. In context of complex earth systems, DA has been long utilised in geosciences, especially in meteorology and weather prediction [2], climate change [3], and more recently in attempting long-term climate prediction [7]. In this paper, we will concentrate on the application of DA to meteorology – often interpreted as accurate forecasts on short time-scales ($\lesssim 2$ weeks), and climate prediction – on time-scales longer than typical range covered by meteorology or weather prediction ($\gtrsim 2$ weeks). In such earth systems, the proposed models are typically dynamic, high-dimensional and qualitatively error-prone due to the inherent complexity in modelling the system. In particular, the dynamic nature of the models result in a discrete and sequential implementation of DA in time [2]; this essentially differentiates DA from a matched-filtering procedure where the model forms are deterministic and incorporate explicit time-dependence.

Theoretically speaking, the complexity – and accuracy – of DA for a given system is shared by the intrinsic complexity in the model form (e.g. model degrees of freedom, participating sub-systems, etc) as well as the nature of observations (e.g. the spatial and temporal scarcity of data points, accuracy of the observational datasets, etc). In practice, however, limitations on DA due to the nature of observational datasets are largely systematic and extrinsic, while the impact of the model form has a more fundamental and profound impact. In this respect, the case of coupled systems is extremely

relevant and interesting since it presents with a realistic challenge where the model form of the system entails two or more sub-components with differing time-scales, e.g. ocean-atmosphere coupled earth system. This has a fundamental impact on the accuracy of DA on each observed sub-component on any intended time-scale and to varying magnitudes [7, 8]. In this paper, we will study the effects of multi-component coupling in the model form on the DA procedure using two toy models capturing the macroscopic properties of ocean-atmosphere interactions – one linear, and one non-linear and chaotic. The intention, in the end, is to develop a zero-order treatment of sequential coupled data assimilation and possible modifications to it in the linear as well as non-linear and chaotic regime.

2 Linear coupled model form

The linear toy model M_{lin} for the first case study is adopted from Barsugli and Battisti [1], which is a simple one-dimensional, thermally coupled, purely temporal and stochastically forced atmosphere-ocean system of the form

$$m \frac{dT_O}{dt} = C_{OO} T_O + C_{OA} T_A, \quad (1)$$

$$\frac{dT_A}{dt} = C_{AO} T_O + C_{AA} T_A + F(t). \quad (2)$$

In matrix form, the coupled system may be written as

$$\nabla \mathbf{T} = \mathbf{C} \mathbf{T} + \mathbf{F}, \text{ where,} \quad (3)$$

$$\nabla = \begin{bmatrix} m \frac{d}{dt} & \emptyset \\ \emptyset & \frac{d}{dt} \end{bmatrix}, \quad \mathbf{T} = \begin{bmatrix} T_A \\ T_O \end{bmatrix},$$

$$\mathbf{C} = \begin{bmatrix} C_{OO} & C_{OA} \\ C_{AO} & C_{AA} \end{bmatrix}, \text{ and } \mathbf{F} = \begin{bmatrix} F(t) \\ \emptyset \end{bmatrix}. \quad (4)$$

where $\mathbf{T} = [T_O, T_A]$ is the state vector of the temperature anomalies in the ocean and atmosphere respectively, matrix \mathbf{C} encodes the exchange of information between the two sub-components, ‘ m ’ encodes the temporal scale separation between the two sub-components, ∇ is the

[†]avneet.singh@uib.no

translation operator and $F(t)$ is the stochastic forcing term. We choose the members of \mathbf{C} and the value of scale separation ‘ m ’ such that the system is stable and in dynamic thermal equilibrium, e.g. $C_{OO} = -0.1$, $C_{OA} = 0.1$, $C_{AO} = 0.01$ and $C_{AA} = -0.1$, and ocean is relatively slow evolving ($m > 1$). The stability of the system is ensured by negative eigenvalues of $\mathbf{C} \leftrightarrow$

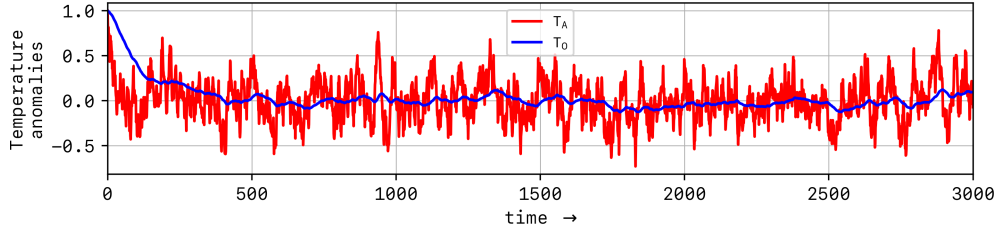


Figure 1: 1-member simulation for $m = 10$, $\sigma_F = 0.1$, and $T_O^{t=0} = T_A^{t=0} = 1.0$.

One may easily calculate the frequency spectrum of the solutions ($t \rightarrow f$) in the Fourier space analytically in this case (5), to quantify the relative slowness of the ocean with respect to the atmosphere; this is shown in figure 2 – the gap between the Fourier transforms \hat{T}_O and \hat{T}_A quantifies the slowness of the ocean relative to the atmosphere.

$$\begin{aligned}\hat{T}_O(f) &= \sigma_F^2 \frac{C_{OA}}{(2\pi i f - C_{AA})(2\pi i m f - C_{OO}) - C_{OA} C_{AO}} \\ \hat{T}_A(f) &= \sigma_F^2 \frac{2\pi i m f - C_{OO}}{(2\pi i f - C_{AA})(2\pi i m f - C_{OO}) - C_{OA} C_{AO}}\end{aligned}\quad (5)$$

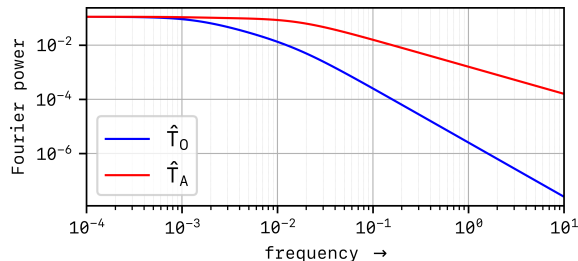


Figure 2: Fourier transforms \hat{T}_O and \hat{T}_A for $m = 10$, $\sigma_F = 0.1$.

Lastly, this temporal scale separation (i.e. slowness of the ocean) leads to a net lagging effect on the ocean which is quantifiable by calculating the auto- and cross-correlation functions (6).

$$\langle T_X, T_Y \rangle \equiv \langle T_X(t), T_Y(t + \tau) \rangle = \int_{-\infty}^{+\infty} T_X(t) T_Y(t + \tau) dt. \quad (6)$$

$|\mathbf{C}| > 0 \leftrightarrow \mathbf{C}$ is positive definite, which also ensures that the Lyapunov exponents are negative. The presence of the forcing term ensures that the model is dynamically spun up to mimic realistic scenarios and its cross-section σ_F is chosen accordingly. In figure 1, we show a sample time series for a single member simulation.

where τ is the *lag time*. In figure 3, we show the auto- and cross-correlation functions plotted for our linear model where the slowness of ocean is again reflected in shallower decline of the oceanic auto-correlation function $\langle T_O, T_O \rangle$ relative to the atmospheric auto-correlation function $\langle T_A, T_A \rangle$. Notably, the cross-correlation function $\langle T_O, T_A \rangle$ peaks at negative value of τ (denoted by τ_p) depicting that the ocean *lags* the atmosphere, or that the atmosphere *leads* the ocean. We intend to use this lag to our advantage in the data assimilation procedure. The statistics of $|\tau_p|$ as a function of scale separation ‘ m ’ are shown in figure 4; we find that the modes of the distributions (i.e. values of $|\tau_p|$) increase with increasing scale separation (i.e. ‘ m ’) as expected. Moreover, while $|\tau_p|$ primarily depends on ‘ m ’ and $|\mathbf{C}|$, the higher moments (skewness, kurtosis, etc) depend on $\mathbf{C} - \text{diag}(\mathbf{C})$.

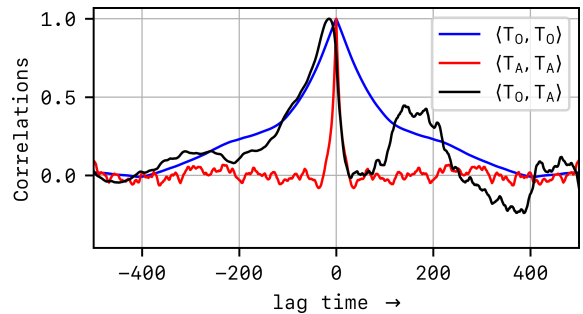


Figure 3: Cross- and auto-correlation functions $\langle T_X, T_Y \rangle$ for a 1-member simulation for $m = 10$, $\sigma_F = 0.1$, and $T_O^{t=0} = T_A^{t=0} = 1.0$. Note that the auto-correlation functions naturally peak at $\tau = 0$ while the cross-correlation peaks at $\tau < 0$ depicting the *lagging effect* on the ocean.

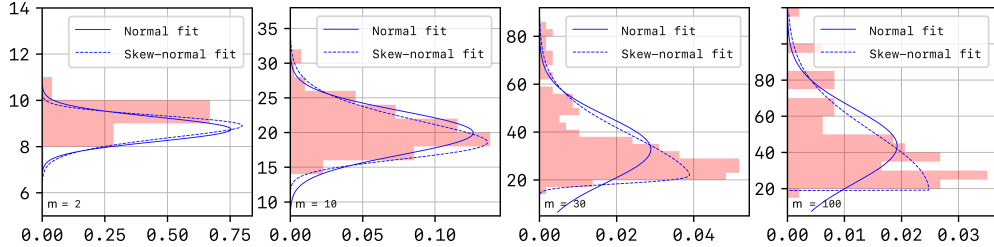


Figure 4: Normalised probability densities (horizontal axes) of peak lag times $|\tau_p|$ (vertical axes) as a function of scale separation ‘ m ’; $\sigma_F = 0.1$, and $T_O^{t=0} = T_A^{t=0} = 1.0$. The solid lines denote normal distribution fits while the dashed lines denote skew-normal fits. Note the shift in the mode, the skewness and the spread of the distributions as a function of increasing values of $m \in \{2, 10, 30, 100\}$.

2.1 Coupled data assimilation

In order to study and optimise data assimilation using this coupled linear model \mathcal{M}_{lin} , we utilise the existing framework of sequential *Ensemble Kalman Filter* (*ab-brev.* EnKF); it is a well known fact that in the linear case, EnKF is the most optimal choice for data assimilation considering the analytical constraints as it equates to a unique and global minimisation of the standard variational approach [2]. If the model error covariance matrix is denoted by \mathbf{P} , the observational error covariance matrix by \mathbf{R} , then the Kalman Gain \mathbf{K} at any time t is written as

$$\mathbf{K}_t = \mathbf{P}_t [\mathbf{P}_t + \mathbf{R}_t]^{-1}. \quad (7)$$

The resulting analysed and forecast state at any time t are further written as

$$\mathbf{T}_t^{\text{ana}} = \mathbf{T}_t^{\text{for}} + \mathbf{K}_t [\mathbf{T}_t^{\text{obs}} - \mathbf{T}_t^{\text{for}}], \quad (8)$$

where $\mathbf{T}_t^{\text{obs}}$ and $\mathbf{T}_t^{\text{for}}$ are the observation and forecast vectors. The analysed model error covariance matrix evolves as $\mathbf{P}_t^{\text{ana}} = \mathbf{P}_t^{\text{for}} [\mathbf{I} - \mathbf{K}_t]$ although this calculation is not required explicitly by the ensemble version

$$\mathbf{K}_t = \frac{1}{D_t} \begin{bmatrix} \langle \vec{T}_A^{\text{for}} | \vec{T}_A^{\text{for}} \rangle [\langle \vec{T}_O^{\text{for}} | \vec{T}_O^{\text{for}} \rangle + \sigma_{O,\text{obs}}^2] - \langle \vec{T}_O^{\text{for}} | \vec{T}_A^{\text{for}} \rangle^2 \\ \sigma_{A,\text{obs}}^2 \langle \vec{T}_A^{\text{for}} | \vec{T}_O^{\text{for}} \rangle \end{bmatrix}$$

where $D_t = [\langle \vec{T}_A^{\text{for}} | \vec{T}_A^{\text{for}} \rangle + \sigma_{A,\text{obs}}^2][\langle \vec{T}_O^{\text{for}} | \vec{T}_O^{\text{for}} \rangle + \sigma_{O,\text{obs}}^2] - \langle \vec{T}_O^{\text{for}} | \vec{T}_A^{\text{for}} \rangle^2$, and $\vec{\cdot}$ represents the ensemble vector of length N_e , the time-varying spread of the ensembles is denoted by $\sigma_{A/O,\text{for/ana}}$, and the $\langle \cdot | \cdot \rangle$ operation represents inner product. Naturally, $\langle \vec{T}_O^{\text{for}} | \vec{T}_A^{\text{for}} \rangle = \langle \vec{T}_A^{\text{for}} | \vec{T}_O^{\text{for}} \rangle$ and that $\langle \vec{T}_X^{\text{for}} | \vec{T}_Y^{\text{for}} \rangle$ is generally equivalent to the discrete formulation of the zero-lag correlation function $\langle T_X, T_Y \rangle_{\tau=0}$ in (6). This completes the required ingredients for EnKF. In table 1, we list the values of the parameters defined above.

of the Kalman filter. The analysed state $\mathbf{T}_t^{\text{ana}}$ is finally translated in time from t to $t+1$ by the translation operation, $\mathbf{T}_{t+1}^{\text{for}} = \mathcal{M}_{\text{lin}} \cdot \mathbf{T}_t^{\text{ana}}$, by numerically integrating the coupled stochastic differential equations¹ (1)–(2). In our experiments, we reasonably assume the observation errors in the ocean and the atmosphere to be mutually uncorrelated and constant in time, i.e.

$$\mathbf{R}_t = \begin{bmatrix} \sigma_{A,\text{obs}} & \emptyset \\ \emptyset & \sigma_{O,\text{obs}} \end{bmatrix}_{\forall t}, \quad (9)$$

while the model error covariance matrix \mathbf{P}_t is explicitly written as

$$\mathbf{P}_t = \begin{bmatrix} \langle \vec{T}_A^{\text{for}} | \vec{T}_A^{\text{for}} \rangle & \langle \vec{T}_A^{\text{for}} | \vec{T}_O^{\text{for}} \rangle \\ \langle \vec{T}_O^{\text{for}} | \vec{T}_A^{\text{for}} \rangle & \langle \vec{T}_O^{\text{for}} | \vec{T}_O^{\text{for}} \rangle \end{bmatrix}_t. \quad (10)$$

The observation vectors for the ocean and the atmosphere in our experiments are generated by perturbing a 1-member simulation of the model \mathcal{M}_{lin} with $\sigma_{O,\text{obs}}$ and $\sigma_{A,\text{obs}}$ respectively. Lastly, the Kalman Gain matrix \mathbf{K}_t is explicitly written as

$$\mathbf{K}_t = \begin{bmatrix} \sigma_{O,\text{obs}}^2 \langle \vec{T}_O^{\text{for}} | \vec{T}_A^{\text{for}} \rangle \\ \langle \vec{T}_O^{\text{for}} | \vec{T}_O^{\text{for}} \rangle [\langle \vec{T}_A^{\text{for}} | \vec{T}_A^{\text{for}} \rangle + \sigma_{A,\text{obs}}^2] - \langle \vec{T}_A^{\text{for}} | \vec{T}_O^{\text{for}} \rangle^2 \end{bmatrix}_t, \quad (11)$$

Parameter	Value	Parameter	Value
m	$\in [1, 21]$	τ	$\in [0, 41]$
$T_O^{t=0}$	0.0	$T_A^{t=0}$	0.0
$\sigma_{O,\text{for}}^{t=0}$	1.0	$\sigma_{A,\text{for}}^{t=0}$	2.0
$\sigma_{O,\text{obs}}$	1.0	$\sigma_{A,\text{obs}}$	2.0
σ_F	1.0	N_e	25

Table 1: Values of the parameters

¹The expression (3) is of the *Ito* form and its numerical integration is performed using `sdeint.itoint` algorithm available in Python’s SciPy library. More specifically, `sdeint.itoint` uses the Euler-Maruyama algorithm to integrate the Ito equation.

We quantify the performance of DA by calculating the RMSE vector defined by

$$\sigma_{\text{RMSE}} = \sqrt{\sum_{\forall t} |\mathbf{T}_t^{\text{ana}} - \mathbf{T}_t^{\text{for}}|^2}. \quad (12)$$

In standard large-scale data assimilation applications, a *fully/strongly* coupled approach (*abbrev.* SCDA) as outlined above is not yet adopted although its application has been encouraged in recent times [6]. The current adoption of *weakly* coupled implementation (*abbrev.* WCDA) simply involves setting the off-diagonal terms

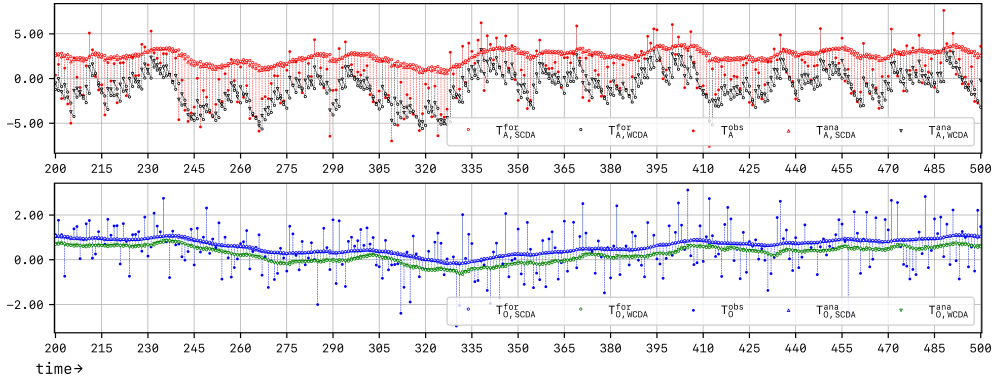


Figure 5: One random member EnKF simulation for $m = 10$ showing the differences between the WCDA and the SCDA implementation. Top panel (red) shows the atmospheric component while the bottom panel depicts the ocean (blue).

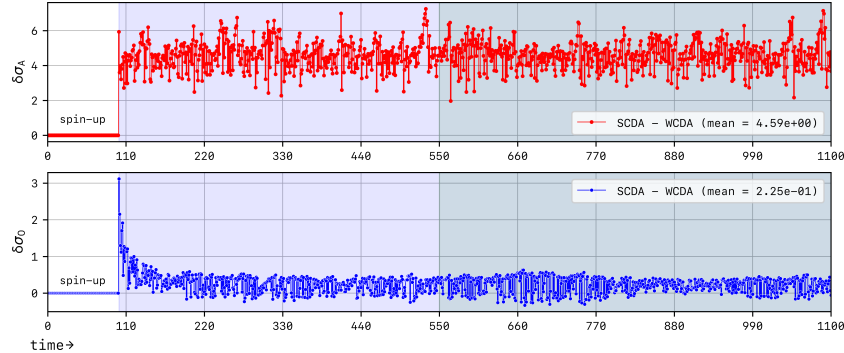


Figure 6: RMSE statistics derived a 25-member EnKF simulation for $m = 10$ showing the difference between the WCDA and the SCDA implementation. The model is spun up to stability during time $t \in [0, 100]$ whereas the RMSE statistics are calculated for time $t \in [550, 1100]$.

2.2 Leading averaged cross-covariance

In order to maximise the effects of cross-covariance in coupled data assimilation, Lu *et al* [4, 5] suggested that it is advantageous to use leading forecasts and observations in the fast sub-component, i.e. the atmosphere, while updating the slower sub-component, i.e. the ocean, instead of assimilating the instantaneously available atmospheric observation at any time t . This suggestion simply follows from figure 3 where we found that the cross-correlation function is maximum when atmosphere leads the ocean, i.e. when $\tau < 0$. This essentially means that the information shared between

in \mathbf{P}_t to zero, thereby explicitly ignoring the model error covariances in the analysis step and only allowing the coupled system to share information during the forecast step; this approach is prone to instabilities. In order to show the difference between the two, we run WCDA simulations in parallel with SCDA in all our experiments and calculate $\delta\sigma_{\text{RMSE}} = \sigma_{\text{RMSE}}^{\text{SCDA}} - \sigma_{\text{RMSE}}^{\text{WCDA}}$. In figure 5, we show a snapshot of a random ensemble member's simulation while figure 6 shows the corresponding RMSE statistics derived from a 25-member EnKF simulation by fixing $m = 10$.

the oceanic and the atmospheric sub-components in the cross-update may be optimised further by choosing $\tau < 0$, thus maximising the signal-to-noise ratio (SNR) in the cross-update. In order to further minimise the effects of noise arising due to stochastic forcing, Lu *et al* [4] used an *average* over some τ_{win} number of leading observations in the atmosphere to update the ocean; they termed this implementation as LACC [4, 5]. Note that no modification was necessary in reverse, i.e. ocean \rightarrow atmosphere, since the faster sub-component doesn't benefit from any such modification directly.

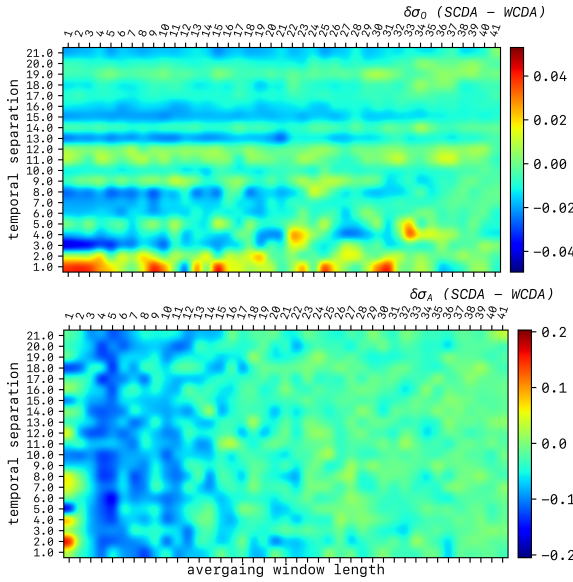


Figure 7: RMSE statistics derived a 25-member EnKF simulation as a function of ‘m’ (vertical axes) and τ_{win} (horizontal axes) showing the difference between the WCDA and the LACC implementation.

In this paper, we will attempt to quantify the effects of choices of τ_{win} on $\delta\sigma_{\text{RMSE}}$. It may be noted that the optimal choice of τ_{win} must depend on ‘m’ since $|\tau_p|$ depends on ‘m’. Consequently, the results of the LACC implementation (compared with WCDA) are shown in figure 7 as a function of ‘m’ and τ_{win} . We note that larger scale separations require longer leading averaging windows in order to maximise the cross-component SNR. Moreover, choosing longer window lengths also decreases the frequency of the fully coupled cross-updates (since the cross-update is made only when preceding τ_{win} observations in the atmosphere become available) which contributes toward decreasing the effect of stochastic noise due to the forcing term.

2.2.1 Inflation and cross-localisation

The effects of stochastic noise due to the forcing term are reduced by the averaging operation yet they are not completely removed. This leaves further room for optimisation of the LACC implementation; this is achieved by adaptively inflating the cross-update by multiplying the error covariance matrix \mathbf{P}_t by a time-dependent factor α_t . In our experiments, it turns out that deflation is required instead of inflation to counter the stochasticity in the atmospheric sub-component. The mean value $\bar{\alpha}_t$ over time of the multiplicative inflationary factor α_t is found to be roughly 0.8. In figure 8, we can see the smoothing effect of inflation on the results of our RMSE statistics. We also find that deflation helps in stricter convergence of LACC implementation for the same reason.

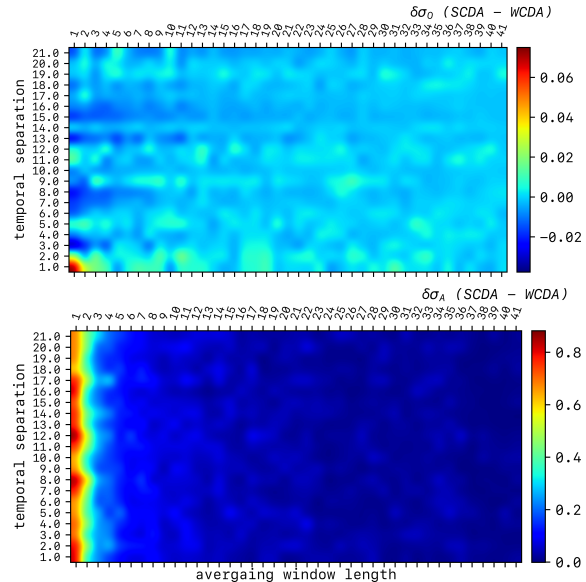


Figure 8: RMSE statistics including adaptive inflation. The mean value $\bar{\alpha}_t$ of the multiplicative adaptive inflationary factor α_t is roughly 0.8 in our experiment.

References

- [1] JJ Barsugli and D S Battisti. *Strongly Coupled Data Assimilation Using Leading Averaged Coupled Covariance (LACC). Part II: CGCM Experiments*. *J. Atmos. Sci.*, 55(–):477–493, 1998.
- [2] A Carrassai *et al.* *Data assimilation in the geosciences: An overview of methods, issues, and perspectives*. *WIREs Climate Change*, 9(5):e535, 2018.
- [3] A Hannart *et al.* *DADA: data assimilation for the detection and attribution of weather and climate-related events*. *Climatic Change*, 136(2):155–174, 2016.
- [4] F Lu *et al.* *Strongly Coupled Data Assimilation Using Leading Averaged Coupled Covariance (LACC). Part I: Simple Model Study*. *Mon. Wea. Rev.*, 143(–):3823–3837, 2015.
- [5] F Lu *et al.* *Strongly Coupled Data Assimilation Using Leading Averaged Coupled Covariance (LACC). Part II: CGCM Experiments*. *Mon. Wea. Rev.*, 143(–):4645–4659, 2015.
- [6] S G Penny and T M Hamill. *Strongly Coupled Data Assimilation for Integrated Earth System Analysis and Prediction*. *Bull. Amer. Meteor. Soc.*, 98(–):ES169–ES172, 2017.
- [7] S G Penny *et al.* *Data assimilation in the geosciences: An overview of methods, issues, and perspectives*. *Journal of Advances in Modeling Earth Systems*, 11(6):1803–1829, 2019.

-
- [8] M Tondeur *et al.* *On temporal scale separation in coupled data assimilation with the ensemble Kalman filter.* *submission in progress* [↗](#), –(–):–, 2019.